EPJ Web of Conferences **40**, 13001 (2013)
DOI: 10.1051/epjconf/20134013001
© Owned by the authors, published by EDP Sciences, 2013

Dynamic magnetic properties of $Fe_{70}Co_{30}$(100) single-crystal thin films deposited at various substrate temperatures

T. Kawai[1], Y. Asai[1], M. Ohtake[1], S. Takeda[2], and M. Futamoto[1]

[1]Faculty of Science and Engineering, Chuo University, 1-13-27 Kasuga, Bunkyo-ku, Tokyo 112-8551, Japan
[2]Magnontech Ltd., 787-16 Jurokken, Kumagaya, Saitama 360-0846, Japan

Abstract. Crystallographic orientation dependence of Gilbert damping constant, α, has been measured under different static magnetic fields for $Fe_{70}Co_{30}$(100) single-crystal thin film samples prepared at various substrate temperatures. Lorentz type resonance peaks are observed for the samples prepared below 200 ºC. For a sample deposited at 400 ºC, broadening of the resonance peak is observed, which is related with an increased surface roughness. α value decreases monotonically with increasing the static field when the field is applied parallel to the easy magnetization axis, whereas it increases when the field is applied along the hard magnetization axis up to around the anisotropy field and then decreases. The minimum value of α is determined to be 0.012 for the hard axis under static fields greater than 650 Oe. The value is twice larger compared with that of Fe(100) single-crystal film. The static magnetization curves measured for $Fe_{70}Co_{30}$ films show large deviations from the curves expected by coherent rotation mode. Such deviation seems to be a possible reason for a larger α value of $Fe_{70}Co_{30}$ thin film.

1 Introduction

Understanding the dynamic magnetization process in magnetic thin films is strongly required for developments of high-frequency magnetic devices such as magnetic recording heads and random access memory devices [1, 2]. Ferromagnetic resonance (FMR) is a useful technique to evaluate dynamic magnetic properties of magnetic thin films. Two types of FMR measurements are widely used. One is the method using a microwave cavity where the FMR line width is measured by sweeping the magnetic filed at a fixed frequency [3, 4]. The other is the method employing a vector network analyser (VNA) where the frequency is swept under a fixed magnetic field [5-7]. Dynamic magnetic properties at arbitrary magnetization states of a sample are important for the actual devices which operate under various magnetic fields [8]. FMR signals are easily observed by using a VNA technique under various magnetic fields. Epitaxial Fe-Co alloy films are widely used in magnetic tunnelling junction devices.

In the present study, dynamic magnetic properties of $Fe_{70}Co_{30}$(100) single-crystal thin film are investigated by broadband FMR employing a VNA [7]. FMR properties are known to be influenced by not only an intrinsic property of magnetic material but also extrinsic factors such as crystallographic defects, surface roughness, etc. [9]. In order to investigate the effect of crystallographic quality on dynamic magnetic properties, $Fe_{70}Co_{30}$ films are prepared by changing the substrate temperature. The dynamic properties are compared with those of Fe(100) single-crystal film in order to clarify the effects of extrinsic factors.

2 Experimental procedures

$Fe_{70}Co_{30}$ (100) single-crystal thin films and an Fe(100) single-crystal film with thickness of 40 nm were prepared by using an UHV-RF magnetron sputtering system equipped with a reflection high energy electron diffraction (RHEED) facility on MgO(100) single-crystal substrates. An $Fe_{70}Co_{30}$ (at. %) alloy target was employed and the substrate temperature for film deposition was varied between RT and 400 ºC. An Fe film was also deposited at 200 ºC by employing an Fe target (>99.9 at. % purity). The film structure was investigated by RHEED and X-ray diffraction (XRD) with Cu-$K\alpha$ radiation (λ=0.15418 nm). The surface morphology was observed by atomic force microscopy (AFM). Static magnetic properties were measured by using a VSM. Inductance measurements were carried out under static magnetic fields applied along [001] and [011] of $Fe_{70}Co_{30}$ single-crystal films, where [001] is the easy magnetization axis while [011] is the hard magnetization axis. A VNA was used to measure dynamic magnetic property covering up to 13 GHz, where RF magnetic field was applied orthogonally to the static magnetic field

This is an Open Access article distributed under the terms of the Creative Commons Attribution License 2.0, which permits unrestricted use, distribution, and reproduction in any medium, provided the original work is properly cited.

using a shorted micro-strip line [7]. The resonant frequency was determined as a frequency when an experimental complex permeability, μ'', showed maximum. Gilbert damping constant, α, was estimated by a fitting of μ'' between experiment and calculation as mentioned in the next section.

3 Analytical model of Polder tensor for (100) single crystal film

Polder tensor [10] is widely used to analyze complex permeability of magnetic film based on Landau-Lifshitz-Gilbert (LLG) equation. However the Polder tensor is not suitable for (100) single-crystal film which has a four-fold symmetry of magnetic anisotropy field. Therefore, a modified model including anisotropy field is developed. In an orthogonal x-y-z coordination, the z-axis is set along a static magnetic field and the film is set in the x-z plane. RF magnetic field is applied in the x-y plane. The LLG equation is expressed using magnetic field, $\boldsymbol{H}_{eff}$, as,

$$\frac{d\boldsymbol{M}}{dt} = -\gamma \cdot \left(\boldsymbol{M} \times \boldsymbol{H}_{eff}\right) + \frac{\alpha}{M_S} \cdot \left(\boldsymbol{M} \times \frac{d\boldsymbol{M}}{dt}\right) \quad , \qquad (1)$$

with $\boldsymbol{H}_{eff}=\boldsymbol{H}-\boldsymbol{H}_{\mathrm{d}}+\boldsymbol{H}_{\mathrm{a}}$, $\boldsymbol{H}=(h_{\mathrm{x}}, h_{\mathrm{y}}, H_{\mathrm{z}})$

, where $\boldsymbol{M}$ is the magnetization of film, γ is gyromagnetic constant, α is Gilbert damping constant, M_{S} is the saturation magnetization of film, $\boldsymbol{H}_{\mathrm{d}}$ is the demagnetization field, $\boldsymbol{H}_{\mathrm{a}}$ is the anisotropy field, h_{x} and h_{y} are radio-frequency magnetic fields along the x and the y direction, and H_{z} is the static magnetic field along z-axis. The solutions of equation (1) are given in the formulae (2) and (3) as,

$$\chi_{xx}' = \frac{\omega_m \cdot \left\{\omega_x \cdot \omega_y{}^2 - \omega_y \cdot \omega^2 \cdot \left(1+\alpha^2\right) + \left(\omega \cdot \alpha\right)^2 \cdot \left(\omega_x + \omega_y\right)\right\}}{\left\{\omega_x \cdot \omega_y - \omega^2 \cdot \left(1+\alpha^2\right)\right\}^2 + \left(\omega \cdot \alpha\right)^2 \cdot \left(\omega_x + \omega_y\right)^2}, \qquad (2)$$

$$\chi_{xx}'' = \frac{\omega_m \cdot \omega \cdot \alpha \cdot \left\{\omega_y{}^2 + \omega^2 \cdot \left(1+\alpha^2\right)\right\}}{\left\{\omega_x \cdot \omega_y - \omega^2 \cdot \left(1+\alpha^2\right)\right\}^2 + \left(\omega \cdot \alpha\right)^2 \cdot \left(\omega_x + \omega_y\right)^2}. \qquad (3)$$

Here, ω values are defined as,

$$\omega_m = \frac{1}{\mu_0} \cdot \gamma \cdot M_S \quad , \quad \omega_i = \gamma \cdot H_z \quad ,$$
$$\omega_x = \omega_i + \omega_m \cdot N_x{}^e \quad , \quad \omega_y = \omega_i + \omega_m \cdot \left(1 + N_y{}^e\right) .$$

For a bcc (100) plane with cubic symmetry,

$$N_x{}^e \cdot \frac{M_S}{\mu_0} = \frac{2K_1}{M_S} \cdot \cos 4\theta \quad , \quad N_y{}^e \cdot \frac{M_S}{\mu_0} = \frac{K_1}{2M_S} \cdot (3 + \cos 4\theta)$$

, where μ_0 is the permeability of vacuum, K_1 is the anisotropy energy of film, θ is the angle of magnetization tilting from [001]. Kittel resonant frequency is given as $\omega_0=\omega_{\mathrm{x}}\times\omega_{\mathrm{y}}$. When $\omega_{\mathrm{x}}=\omega_{\mathrm{y}}$, the formulae (2) and (3) are in agreement with the Polder tensor. Fitting parameters are M_{s}, K_1, γ, θ, and α. The values calculated by using the formula (3) are compared with the experimental value of μ''.

4 Results and discussion

4.1 Structure analyses

The RHEED pattern observed for an $Fe_{70}Co_{30}$ film deposited on MgO(100) substrate was corresponding to bcc(100) texture, similar to the cases of Fe and $Fe_{50}Co_{50}$ deposition reported previously [11]. Single-crystal thin films were obtained for all of the substrate temperatures. The epitaxial orientation relationship is determined as,

$Fe_{70}Co_{30}(100)[011]_{\mathrm{bcc}} \parallel MgO(100)[001]_{B1}$.

In this configuration, the lattice mismatch between $Fe_{70}Co_{30}(100)$ and MgO(100) lattices calculated by citing the lattice constants of bulk materials, is –3.7%. The lattice spacings of $Fe_{70}Co_{30}$ films using the bcc(200) reflections obtained by the out-of-plane (out) and the in-plane (in) XRD spectra are listed in Table 1 together with the $\Delta\theta_{50}$ values of rocking curves. The lattice spacings estimated from the reflection peaks are in agreement with the values of bulk $Fe_{70}Co_{30}$ crystals with very small errors less than ±0.2%. The values of $\Delta\theta_{50}$ are less than 1.0 degree. The XRD results indicate that the film strains are small. The AFM images of $Fe_{70}Co_{30}$ films are shown in Fig. 1. The film deposited at RT shows very flat surface with the R_{a}=0.25 nm. However with increasing the deposition temperature, R_{a} increases to 0.39 nm (200 ºC), and 2.14 nm (400 ºC). Many deep holes around 20 nm in depth are observed for the film deposited at 400 ºC. Such surface roughness is expected to give some influence on the dynamic magnetization properties [9].

Table 1. Lattice spacing and $\Delta\theta_{50}$ values of $Fe_{70}Co_{30}$ films.

Sub. temp.	d_{200} (nm)		Error (%)		$\Delta\theta_{50}$ (deg.)	
	Out	In	Out	In	Out	In
RT	0.2863	—	–0.048	—	0.911	—
200 ºC	0.2867	0.2864	0.100	–0.016	0.767	0.669
400 ºC	0.2869	—	0.184	—	0.721	—

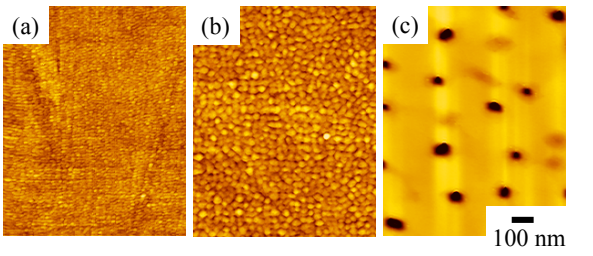

Fig. 1. AFM images of $Fe_{70}Co_{30}$ epitaxial thin films deposited at (a) RT, (b) 200 ºC, and (c) 400 ºC.

4.2 Static magnetic properties

Magnetization curves for $Fe_{70}Co_{30}(100)$ thin films and an Fe(100) thin film are shown in Fig. 2. All the films are easily magnetized when the magnetic field is applied along [001]. Anisotropy fields, H_{a}, estimated from the in-plane magnetization curves are indicated in Fig. 2 for these magnetic films. The H_{a} of $Fe_{70}Co_{30}$ film deposited at RT is 110 Oe. The value is smaller than those deposited at 200 ºC (H_{a} =190 Oe) and 400 ºC (150 Oe). The magnetization curves of $Fe_{70}Co_{30}(100)$ thin films are not closed even under applied fields grater than the

respective anisotropy fields. For example, for the film deposited at RT, the applied field when the magnetization curve is closed is 750 Oe, which is about 7 times larger than the anisotropy filed. Similar tendency is observed for the films deposited at 200 ºC and 400 ºC. The feature indicates that the magnetization process of $Fe_{70}Co_{30}$(100) thin film is different from a coherent rotation mode. For comparison, the magnetization curves of 40nm-thick Fe(100) film prepared at 200 ºC are also shown in Fig. 2 (d). The anisotropy field is 500 Oe. The magnetization curve is closed under an applied field of 100 Oe, which is much smaller than the anisotropy field. Therefore, the magnetization process of Fe(100) thin film is apparently following a coherent rotation mode.

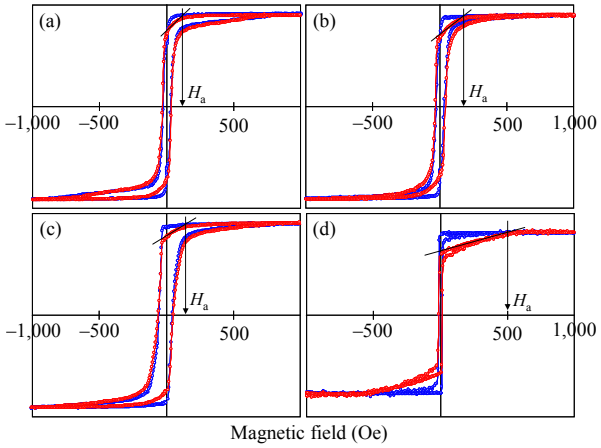

Fig. 2. Magnetization curves measured for $Fe_{70}Co_{30}$ films deposited at (a) RT, (b) 200 ºC, (c) 400 ºC, and (d) for Fe film deposited at 200 ºC. Blue dots are along [001] and red dots along [011]. The magnetization is normalized.

4.3 Dynamic magnetic properties

Figure 3 shows the complex permeability for $Fe_{70}Co_{30}$ films measured under a static magnetic field of 350 Oe applied along the easy axis [001] and the hard axis [011] directions. Lorentz type resonance peaks are observed for the samples prepared below 200 ºC. For the sample prepared at 400 ºC, a broadening of the resonance peak is observed, which seems to be related with the increased surface roughness. The resonance frequency measured along [001] for the film deposited at RT is lower than that of the film deposited at 200 ºC, which indicates that the anisotropy filed increases with increasing the deposition temperature. The shape variation of complex permeability in Fig. 3 suggests that an extrinsic property is giving an influence on the dynamic magnetization property.

Figure 4 shows the effect of static magnetic field on resonant frequency, when the field is applied along the easy axis of [001] and also along the hard axis of [011]. The difference of magnetic field measured along [001] and [011] for a resonant magnetic field corresponds to the anisotropy field. The anisotropy fields of the samples prepared at RT, 200 ºC, and 400 ºC are 116 Oe, 245 Oe, and 320 Oe, respectively. These anisotropy fields evaluated by dynamic magnetic properties are compared

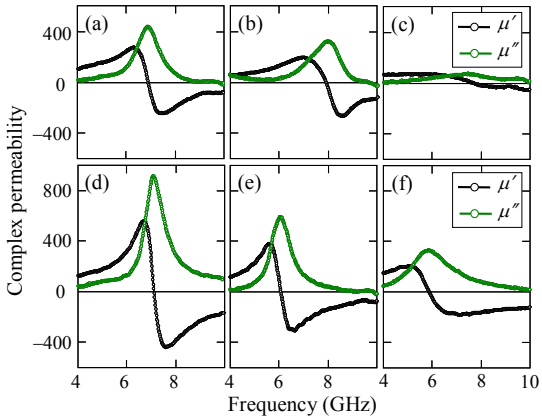

Fig. 3. Complex permeability variations for $Fe_{70}Co_{30}$(100) thin films prepared at (a) (d) RT, (b) (e) 200 ºC, and (c) (f) 400 ºC measured under a static magnetic field of 350 Oe applied along (a) – (c) [001] and along (d) – (f) [011].

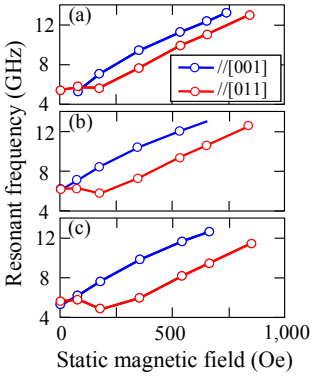

Fig. 4. Static magnetic field dependence of resonant frequency measured for $Fe_{70}Co_{30}$ films deposited at (a) RT, (b) 200 ºC, and (c) 400 ºC.

with those evaluated from the static magnetization curves in Fig. 2. There is no much difference for the samples deposited at RT. On the contrary, the anisotropy field of film deposited at 400 ºC determined from dynamic magnetic property is twice as large as that determined from the magnetization curve. The dynamic magnetization is apparently influenced by an extrinsic property, possibly by the deep holes existing in the film.

Figure 5 shows μ'' measured for an $Fe_{70}Co_{30}$ film deposited at 200 ºC under static magnetic fields up to 654 Oe applied along the [001] and the [011] directions. Solid lines in the figure are the fitted curves calculated by using the formula (3). Damping constant, α, is determined by best fitting between experiments and calculations. There are some discrepancies between experiments and calculations when fields are applied along [001]. These discrepancies indicate that the magnetization process of the films is apart from a coherent rotation and a uniform precession mode. In Fig. 6, μ'' characteristics measured for an Fe(100) single-crystal film are shown. Better agreements between experiments and calculations are recognized for the Fe thin film, which indicates that dynamic magnetization of Fe film is following a uniform precession mode. Figure 7 shows the static magnetic field dependence of damping constant measured for the $Fe_{70}Co_{30}$ and the Fe single-crystal thin films deposited at

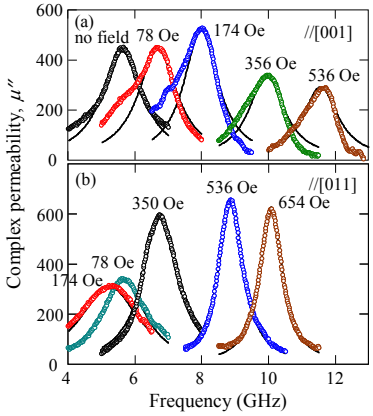

Fig. 5. Complex permeability, μ'', for an $Fe_{70}Co_{30}$ film prepared at 200 ºC measured under different static magnetic fields applied along (a) [001] and (b) [011]. Solid lines are the fitted curves.

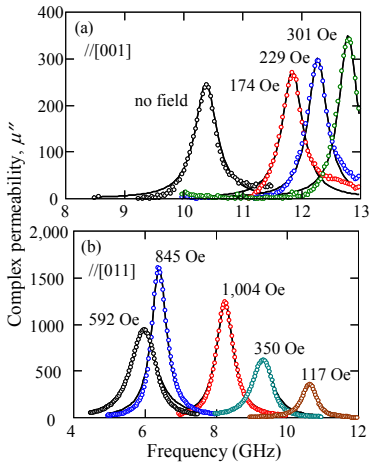

Fig. 6. Complex permeability, μ'', for an Fe film prepared at 200 ºC measured under different static magnetic fields applied along (a) [001] and (b) [011]. Solid lines are the fitted curves.

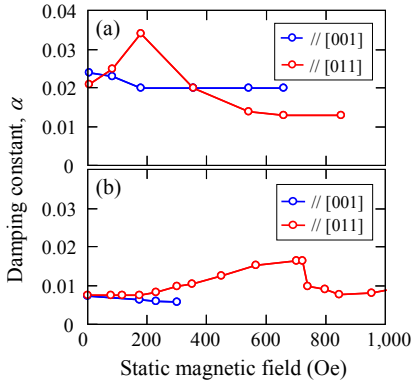

Fig. 7. Dependence of damping constant, α, on static magnetic field estimated for (a) $Fe_{70}Co_{30}$ and (b) Fe films prepared at 200 ºC.

200 ºC. For the $Fe_{70}Co_{30}$ film, α value decreases monotonically with increasing the static field when the field is applied along [001], whereas it increases when the field is applied along [011] up to around the anisotropy field and then decreases. The minimum value of α is estimated to be 0.012 along [011] within the present experimental condition. For the Fe film, the static magnetic field dependence of α is similar to that of $Fe_{70}Co_{30}$ film case. The minimum value of α is 0.006 along [001], which is much smaller than that of $Fe_{70}Co_{30}$ film. When the Kittel resonant condition is considered, a higher resonant frequency is related with a higher effective field which aligns magnetic moment of the material. Thus the minimum α value is expected at a higher resonant frequency region. This interpretation seems to be applicable for the Fe film, but it is not the case for the $Fe_{70}Co_{30}$ film. Some influence from extrinsic property needs to be considered to explain the dynamic magnetization property. As shown in Fig. 2, the static magnetization curves measured for $Fe_{70}Co_{30}$ films show large deviations from the curves expected by coherent rotation mode, which suggest some anisotropy dispersions are existing in the films. Such anisotropy dispersion may disturb the uniform precession mode. The disturbance of uniform precession seems to be a possible reason for larger α value of $Fe_{70}Co_{30}$ thin film as an extrinsic property contribution.

5 Summary

Dynamic magnetic properties of $Fe_{70}Co_{30}$(100) single-crystal thin films were investigated by using a broad-band FMR technique compared with that of an Fe(100) single-crystal thin film. The α value of $Fe_{70}Co_{30}$ single-crystal film is much larger than that of Fe single-crystal film. The static magnetization curves measured for $Fe_{70}Co_{30}$ film show large deviations from those expected by coherent rotation mode. Such deviation suggests a nonuniform precession of magnetic spins in the film, and seems to be a possible reason for a larger α value of $Fe_{70}Co_{30}$ thin film.

Acknowledgement

We wish to thank Hitachi Metals Ltd. for supporting this work. We also thank Dr. H. Suzuki of KEYCOM Corp. for his kind advice in the broadband FMR measurements.

References

1. J.-G. Zhu, X. Zhu, and Y. Tang, *IEEE Trans. Magn.*, **44**, 125 (2008).
2. J. C. Slonczewski, *J. Magn. Magn. Mater.*, **159**, L1 (1996).
3. F. Schreiber, J. Pflaum, Z. Frait, Th. Muhge, and J. Pelzl, *Solid State Commun.*, **93**, 965 (1995).
4. N. Inaba, H. Asanuma, S. Igarashi, S. Mori, F. Kirino, K. Koike, and H. Morita, *IEEE Trans. Magn.*, **42**, 2372 (2006).
5. V. Bekker, K. Seemann, and H. Leiste, *J. Magn. Magn. Mater.*, **270**, 327 (2004).
6. G. Counnil, J-V. Kim, K. Shigeto, Y. Otani, T. Devolder, P. Crozat, H. Hurdequint, and C. Chappert, *J. Magn. Magn. Mater.*, **272-276**, 290 (2004).
7. S. Takeda and H. Suzuki, *J. Magn. Soc. Jpn.*, **33**, 171 (2009).
8. P. Gelin and K. Berthou-Pichavant, *IEEE Trans. Magn.*, **45**, 1185 (1997).
9. B. K. Kuanr, R. E. Camley, and Z. Celinski, *J. Magn. Magn. Mater.*, **286**, 276 (2005).
10. D. Polder, *Phil. Mag.*, **40**, 99 (1949).
11. K. Matsubara, M. Ohtake, F. Kirino, and M. Futamoto, *J. Phys.: Conf. Ser.*, **303**, 012093 (2011).